



Responses of polar energy budget to regional SST changes in extra-polar regions

Qingmin Wang¹, Yincheng Liu¹, Lujun Zhang¹, Chen Zhou^{1,*}

¹School of Atmospheric Science, Nanjing University, Nanjing, 210000, China

5 *Correspondence to:* Chen Zhou (czhou17@nju.edu.cn)

Abstract. Surface temperature at polar regions is not only affected by local forcings and feedbacks, but also depends on teleconnections between polar regions and low latitude regions. In this study, the responses of energy budget in polar regions to remote SST changes are analysed using a set of idealized SST patch experiments. The results show that responses of polar energy budget to remote sea surface warmings are regulated by changes in atmospheric energy transport, and radiative
10 feedbacks also contribute to the polar energy budget at both the top-of-atmosphere (TOA) and surface. An increase of poleward atmospheric energy transport to polar regions results in an increase of surface and air temperature, leading to a radiative warming at surface and radiative cooling at TOA. In response to sea surface warmings in most midlatitude regions, the poleward atmospheric energy transport to polar regions in the corresponding hemisphere increases. Sea surface warming over most tropical regions enhances the polar energy transport to both Arctic and Antarctic regions, except that an increase in the
15 Indian Ocean's temperature results in a decrease in poleward atmospheric energy transport to the Arctics due to different responses of stationary waves. Sensitivity of Arctic energy budget to tropical SST changes is generally stronger than that of Antarctic energy budget, and poleward atmospheric heat transport is dominated by dry static energy, with a lesser contribution from latent heat transport. Polar energy budget is not sensitive to SST changes in most subtropical regions.

1 Introduction

20 As global surface temperature increases, the Arctic region has experienced a surface temperature rise more than twice the global average (Lenssen et al., 2019), a phenomenon known as "Arctic Amplification" (AA). AA exemplifies the broader phenomenon of polar amplification, which is also applicable to the Antarctic. However, due to factors such as the higher average elevation of the Antarctic continent, its lower albedo, and feedback efficiency differences, as well as the Southern Ocean's heat absorption capacity (Salzmann, 2017; Hahn et al., 2021), the warming in Antarctica appears more moderate
25 compared to the Arctic (Marshall 2015; Smith, 2019).

The polar energy budget (PEB) is highly sensitive to various local feedback mechanisms. One important mechanism is the ice-albedo feedback. Climate warming reduces polar region snow cover, leading to more solar radiation being absorbed, which in turn accelerates climate warming and further decreases albedo (Dickinson et al., 1987; Hall, 2004; Boeke and Taylor, 2018; Duan et al., 2019). This feedback mechanism forms a positive feedback loop, making the warming in the Arctic more



30 pronounced compared to other regions. Additionally, temperature feedback is another significant contributor to AA (Pithan and Mauritsen, 2014; Laïné et al., 2016; Sejas and Cai, 2016). Temperature feedback manifests as increased downwelling longwave radiation due to atmospheric warming, which in turn heats the surface and increases upwelling longwave radiation, creating a positive feedback loop that amplifies surface and atmospheric warming (Sejas and Cai 2016; Vargas et al., 2019). During climate warming, the transformation of ice clouds into water clouds increases cloud albedo, leading to negative
35 feedback (Mitchell et al., 1989; Li and Le Treut, 1992). Simultaneously, the decrease in lower tropospheric stability increases Arctic cloud cover and optical thickness (Barton et al., 2012; Solomon et al., 2014; Taylor et al., 2015; Yu et al., 2019), contributing to Arctic autumn and winter warming (Boeke and Taylor, 2018). These local feedback mechanisms collectively enhance Arctic warming.

However, polar climate is not only influenced by local feedback processes, but is also highly sensitive to remote effects (Li et al., 2021). Specifically, meridional atmosphere heat transport (AHT) plays a crucial role in polar temperatures (Budyko, 1969; Sellers, 1969; North, 1975), and the efficiency of heat transfer from low latitude regions to the poles significantly surpasses that from high latitude regions to the equator under global warming (Alexeev et al., 2005; Chung and Räisänen, 2011; Park et al., 2018; Shaw and Tan, 2018; Stuecker et al., 2018; Semmler et al., 2020). Multiple global climate model experiments have been conducted to measure the remote influence on Arctic warming. These experiments include adding additional energy terms
45 directly to the surface energy balance (Alexeev et al., 2005; Park et al., 2018), using latitude-restricted increases in CO₂ (Chung and Räisänen, 2011; Shaw and Tan, 2018; Stuecker et al., 2018; Semmler et al., 2020), and specifying increases in sea surface temperature (SST) in low-latitude regions (Yoshimori et al., 2017). These studies indicate that a portion of Arctic warming is induced by indirect effects of remote warming. It is estimated that 50%-85% of Arctic warming is induced by non-local drivers (Chung and Räisänen, 2011; Yoshimori et al., 2017; Park et al., 2018; Shaw and Tan, 2018; Stuecker et al., 2018). Local Arctic
50 feedbacks further amplify this remotely induced Arctic warming, resulting in the final remotely induced warming, accounting for half or more of the total Arctic warming.

In low-latitude regions, sea surface temperature (SST) variations markedly affect the PEB (Alexeev, 2005). It is widely accepted that planetary waves play a critical role in establishing teleconnections between tropical oceans and polar regions. These waves are pivotal in the transport of heat and moisture to the Arctic, consequently driving the increase in polar
55 temperatures (Graversen and Burtu, 2016; Baggett and Lee, 2017). For instance, intensified convective activity within the Pacific Warm Pool not only strengthens the propagation of Rossby waves toward the poles but also increases the frequency of these fluctuations. This enhancement in Rossby wave activity boosts the transport of water vapor to the Arctic, augmenting the downward longwave radiation in the Arctic regions (Rodgers et al., 2003; Lee et al., 2011; Lee, 2012; Lee, 2014). While synoptic-scale waves also contribute to the transport of heat and moisture to the Arctic, their overall impact is relatively minor
60 and becomes significant mainly in the context of amplified planetary waves (Baggett and Lee, 2017). Atmospheric circulation models reveal that warming of tropical SST from glacial to interglacial periods significantly elevates summer temperatures in regions where the Canadian ice sheet forms. This high-latitude response arises from small-amplitude extra-annular climate changes, which alter the vertical distribution of atmospheric temperature and water vapor in the extra-annular zone, primarily



through atmospheric bridging mechanisms. Conversely, cold tropical SST variations exert a lesser impact on water vapor transport and temperature in the Canadian region (Rodgers et al., 2003). The "Tropical Excitation of Arctic Warming Mechanisms" (TEAM) further elucidates this phenomenon: increased polar moist static energy transport during La Niña episodes leads to Arctic winter surface warming, whereas the opposite is true during El Niño episodes (Lee, 2011; 2012; 2014). Analysis of El Niño and La Niña composite data shows that localized tropical convective heating intensifies polar temperature anomalies.

In previous researches, scholars primarily focused on the impact of SST over a large area of tropical oceans on the PEB. However, studies have indicated significant variations in the effects of SST anomalies in different oceanic regions on the global climate system (Barsugli, 2002; Fletcher, 2011). In this study, we employ a set of idealized SST patches experiments to perform a systematic analysis on the response of the PEB to SST changes in various areas.

2 Data and Method

2.1 Individual patch experiments

The patch experiments were conducted using the Community Earth System Model version 1.2.1 integrated with the Community Atmospheric Model 5.3 (CESM1.2.1-CAM5.3, Neale et al. (2012)), operating at a spatial resolution of 1.9° latitude by 2.5° longitude. The experimental setup included a control experiment and two sets of patch experiments—one with warm patches and another with cold patches. The control experiment spanned 41 years, maintaining the sea surface temperature (SST), sea ice, and climatic forcings at the constant present-day levels observed in the (year 2000). The global ocean was segmented into 80 overlapping rectangular areas, comprehensively covering the global ice-free ocean surface, as depicted in Figure 1 of Zhou et al. (2020). In the warm patch experiments, a positive SST anomaly was introduced at the ocean surface within a designated patch, while the SST in other regions is same as the control setup. Conversely, the cold patch experiments involved introducing a negative SST anomaly at the ocean surface within the respective patches. The SST anomalies in each patch were designed according to the equation proposed by Barsugli and Sardeshmukh (2002), which effectively mitigates nonlinearity due to unrealistic SST gradients, ensuring a more realistic simulation of oceanic temperature variations,

$$\Delta SST_p(lat, lon) = A \cos^2\left(\frac{\pi}{2} \frac{lat - lat_p}{lat_w}\right) \left(\frac{\pi}{2} \frac{lon - lon_p}{lon_w}\right), \quad (1)$$

where $|lat - lat_p| < lat_w$, $|lon - lon_p| < lon_w$. The terms lat_p and lon_p are the latitude and longitude of the center point for a specific patch, respectively; lat_w and lon_w are the meridional and zonal half-width of the patch, respectively, with their values set to $lat_w = 10^\circ$ and $lon_w = 40^\circ$ in these experiments; and A is the amplitude of the SST anomaly.

In this study, we analyzed the responses of polar TOA radiation (R_{TOA}), polar surface radiation (R_{sfc}), and meridional atmospheric advection to the polar regions (R_{adv}). The equations for calculating these parameters are listed as follows:

$$R_{TOA} = FSNT - FLNT, \quad (2)$$



$$R_{sfc} = FSNS - FLNS - SH - LH , \quad (3)$$

95 $R_{adv} = R_{sfc} - R_{toa} , \quad (4)$

where $FSNT$ represents the net downward shortwave radiation at the TOA, $FLNT$ denotes the net upward longwave radiation at the TOA, $FSNS$ is the net downward shortwave radiation at the surface, $FLNS$ represents the net upward longwave radiation at the surface, and SH and LH account for the sensible and latent heat fluxes, respectively.

2.2 EOF-SST experiments

100 To quantify the PEB response to realistic SST anomaly patterns, we applied EOF analysis to historical SST data from 1980 to 2019, and identified the first eight EOF modes. We then conducted eight separate EOF-SST experiments, and the SST of each experiment was perturbed by a specific EOF mode relative to the control run. These experiments allow us to isolate and understand the impact of realistic SST anomaly patterns on the PEB.

3 Result

105 3.1 Responses of PEB to Local SST Changes

The differences of annual PEB in conjugate SST patch warming experiments and SST cooling experiments are shown in Figure 1. The location of each point denotes the center of corresponding patch, and the colors of these points denote the differences of PEB between corresponding conjugate warming and cooling patch experiments. Additionally, t-tests were conducted to assess their statistical significance.

110 Figure 1(a) shows the response of Arctic TOA radiation (R_{TOA}) to global ocean warming. Significant changes are noted primarily in patches located in the tropical Indian Ocean and the eastern tropical Pacific. The response of Arctic ΔR_{TOA} to SST warmings in the eastern tropical Pacific is negative, whereas the Arctic ΔR_{TOA} response to warmings in the tropical Indian Ocean is positive. Additionally, there are several patches in the tropical Atlantic and near Antarctica contribute a negative Arctic R_{toa} anomaly. Figure 1(b) depicts the Arctic surface radiation response (R_{sfc}) to global ocean warming. Significant
115 changes can be found in patches located in the tropical Pacific and the tropical Indian Ocean. The response of R_{sfc} to warming in the tropical Pacific and the northwestern tropical Indian Ocean is positive, while the response to warming in the southeastern tropical Indian Ocean is negative. Figure 1(c) shows the response of meridional atmospheric advection near 60°N (R_{adv}) to global ocean warming. Similar to the R_{sfc} response, significant responses can be found in patches located in the tropical Pacific and the tropical Indian Ocean. The response of R_{adv} to warming in the tropical Pacific and the northwestern tropical Indian
120 Ocean is positive, while the response to warming in the southeastern tropical Indian Ocean is negative.

Figure 1(d-f) illustrates the Antarctic R_{TOA} , R_{sfc} and R_{adv} response to global ocean warming. The response of ΔR_{toa} to warming in the tropical Indian Ocean, tropical Pacific Ocean, and Southern Ocean is negative, while the response to warming



in the tropical Atlantic is positive. The response of ΔR_{sfc} to warmings in most tropical regions and part of the Southern Ocean is positive, while the response of ΔR_{sfc} to warmings around 60°S is negative. The response of ΔR_{adv} to warmings in the tropical Indian Ocean, tropical Pacific Ocean, and part of the Southern Ocean is positive.

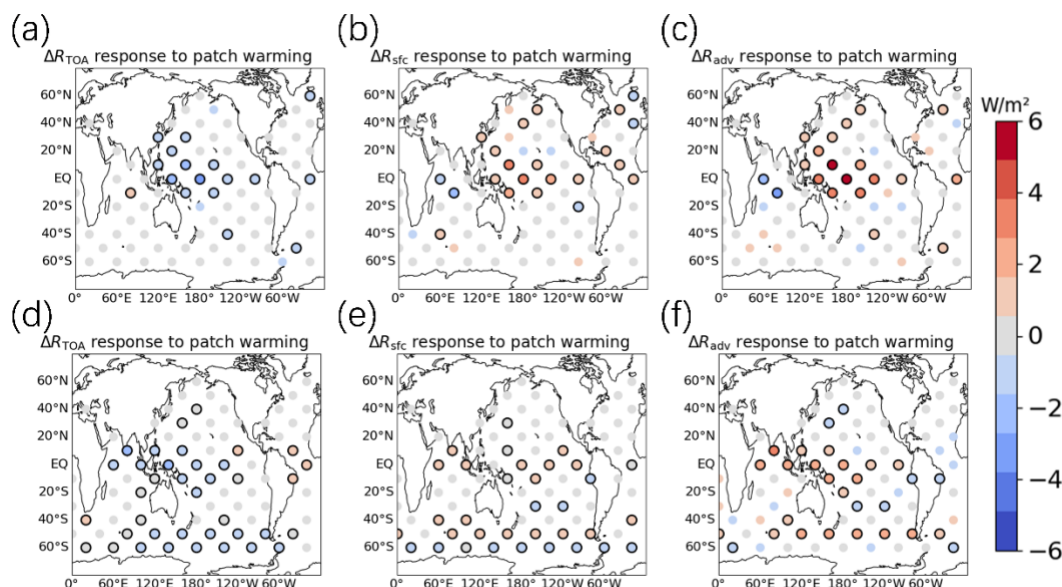


Figure 1: Responses of polar energy budget to regional SST changes. (a) Differences of Arctic (60°N-90°N) annual mean ΔR_{TOA} between conjugate warming and cooling patch experiments. (b) Differences of Arctic annual mean ΔR_{sfc} , (c) Differences of ΔR_{adv} at 60°N. (d-e) Responses of ΔR_{TOA} , ΔR_{sfc} , and ΔR_{adv} in the Antarctic regions. The location of each point denotes the center of corresponding patch, and the colors denotes the differences between conjugate warming and cooling patch experiments. Black circles denote that the differences are statistically significant at 95% confidence level.

The responses of PEB depend on the season. The spatial distribution of the Arctic PEB (Figure 2a-c) response to regional SST in boreal winter (DJF) is similar to the annual average values (Figure 1a-c), but the magnitude of DJF responses is greater than annual responses. For the Antarctic regions, the response of DJF PEB to tropical ocean warming aligns with the annual average.

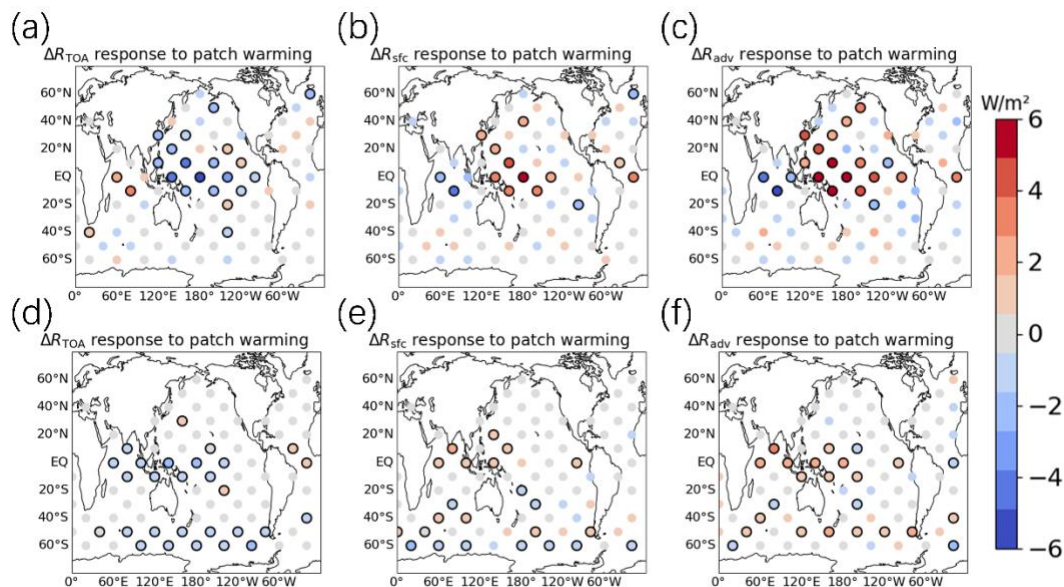


Figure 2: Similar to Figure 1, but for the DJF season.

During boreal summer (JJA), the spatial distribution of Arctic PEB responses (Figs. 3a-c) differ from the annual average. Specifically, the responses of ΔR_{adv} to warmings in both the eastern Indian Ocean and western Pacific Ocean are positive. The responses of ΔR_{sfc} and ΔR_{TOA} in most patch experiments are statistically insignificant. Conversely, the Antarctic PEB responses to tropical ocean warming in JJA are similar to annual mean values.

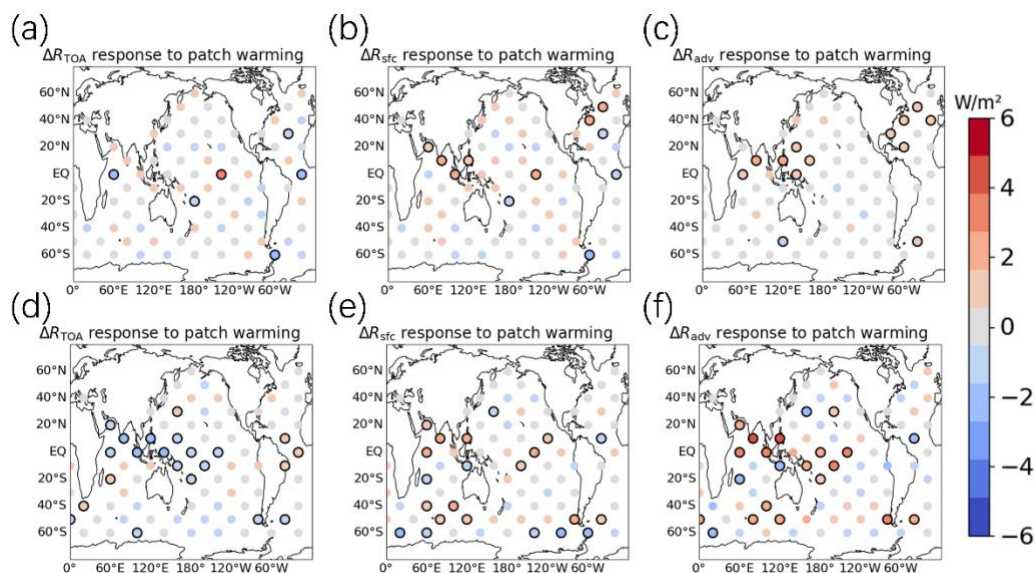




Figure 3: Same as Figure 1, but for the JJA season.

145

To understand the mechanism how PEB is affected by remote SST, we quantify the contributions of meteorological factors to PEB responses (Figures. 4-5) using radiative kernels (Huang et al. 2017).

Figure 4a shows that the contribution of cloud is small to the Arctic ΔR_{TOA} response. Albedo makes an insignificant contribution to Arctic ΔR_{TOA} response for most cases, which is positive in both the tropical Indian Ocean and the Pacific $\Delta R_{TOA,alb}$ (Figure 4b). The impact of Arctic $\Delta R_{TOA,Ta}$ exhibits a positive response to SST increases in the tropical Indian Ocean and a negative response to the tropical Pacific (Figure 4c), indicating that Ta is the primary contributor to Arctic ΔR_{TOA} . The sensitivity of Arctic $\Delta R_{TOA,Ts}$ only responds to increases in the SST of the tropical eastern Pacific, with a negative response. (Figure 4d).

For the Antarctic, the contributions of cloud to ΔR_{TOA} responses are relatively small, despite that the response of $\Delta R_{TOA,clld}$ to SST warming in tropical Pacific Ocean and the Southern Ocean are statistically significant (Figure 4e). The contribution of albedo changes is also small to the response of Antarctic ΔR_{TOA} (see Figure 4f). Similar to the Arctic, Antarctic $\Delta R_{TOA,Ta}$ shows significant responses to regional SST changes, indicating air temperature change is the main contributor to Antarctic ΔR_{TOA} . In response to SST increase in the tropical Indian Ocean and eastern tropical Pacific, Antarctic $\Delta R_{TOA,Ta}$ is negative, while the response is positive to SST increase in the western tropical Pacific and tropical Atlantic (Figure 4g). Surface temperature also contributes to Antarctic ΔR_{TOA} (Figure 5h), but the contribution of surface temperature change is less than that of air temperature change.

160

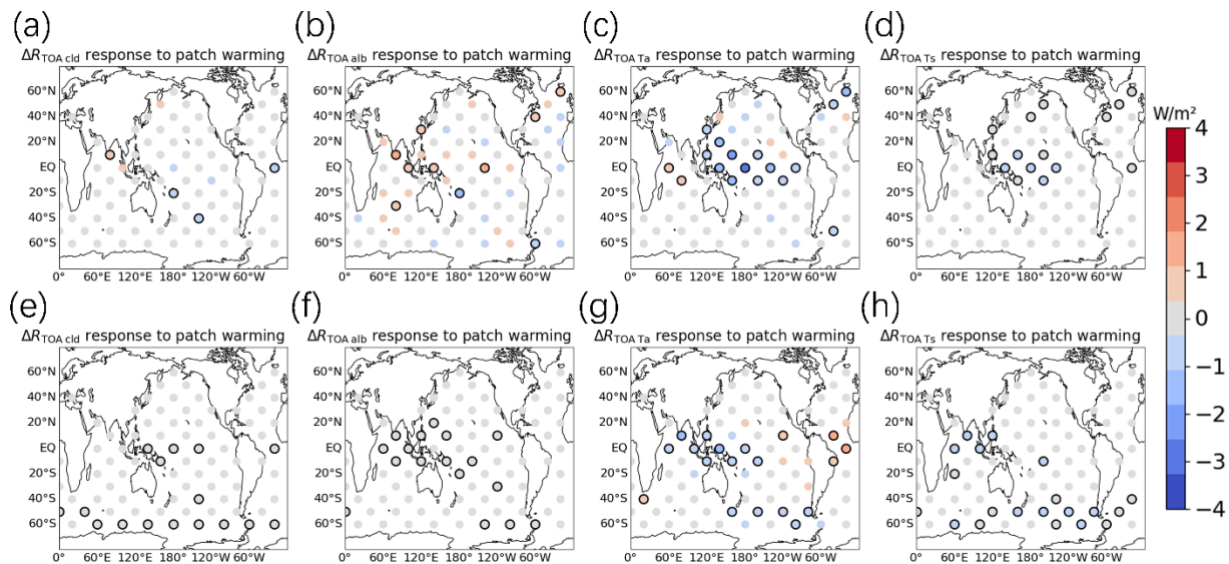


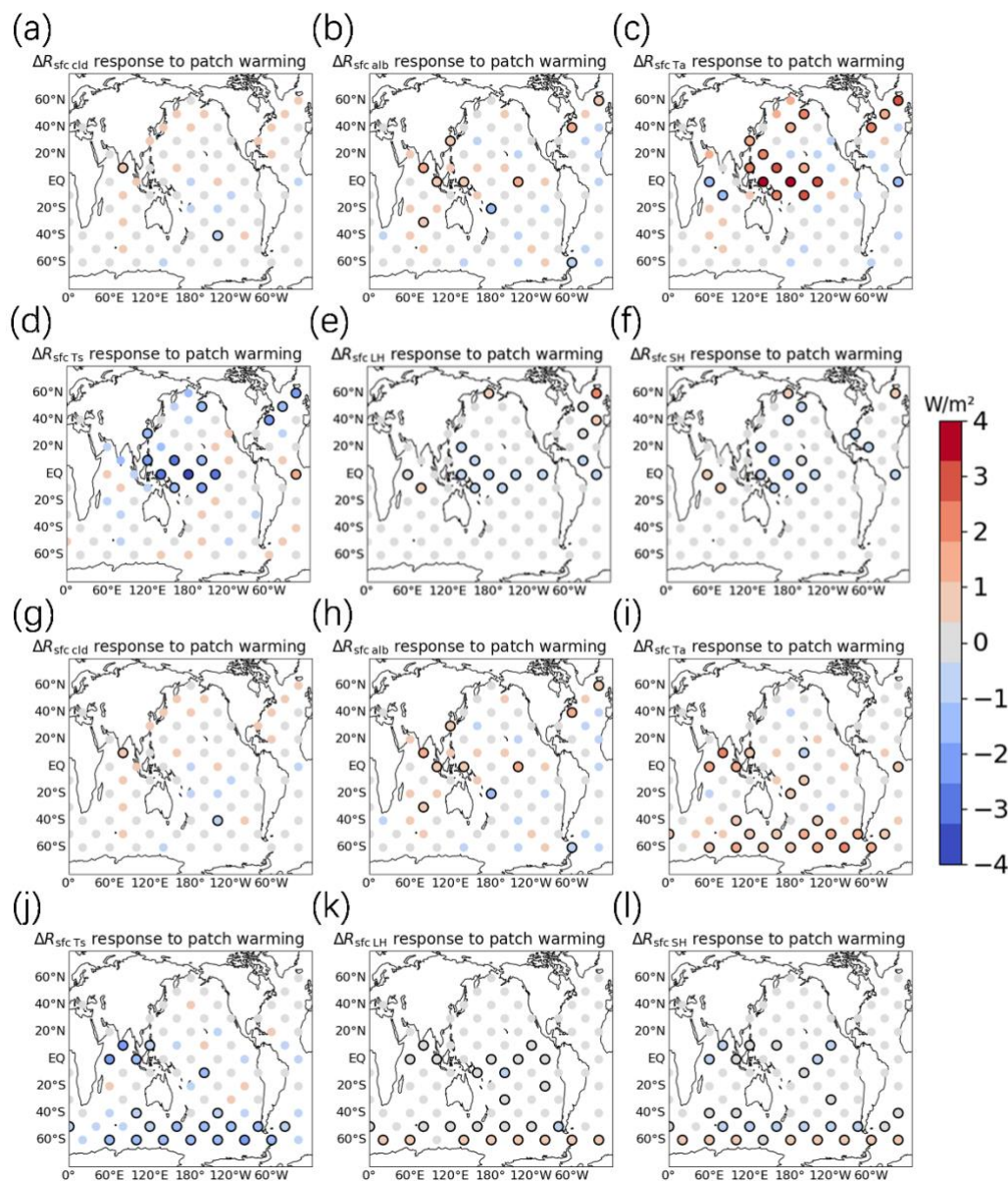
Figure 4: Difference of annual mean $\Delta R_{TOA,clld}$ (a), $\Delta R_{TOA,alb}$ (b), $\Delta R_{TOA,Ta}$ (c), $\Delta R_{TOA,Ts}$ (d) for Arctic and annual mean $\Delta R_{TOA,clld}$ (e), $\Delta R_{TOA,alb}$ (f), $\Delta R_{TOA,Ta}$ (g), $\Delta R_{TOA,Ts}$ (h) for Antarctica between conjugate warming and cooling patch experiments.



165

Figure 5 shows the contributions of meteorological factors to the responses of Arctic and Antarctic ΔR_{sfc} . For the Arctic, clouds have negligible contribution to Arctic ΔR_{sfc} (Figure 5a). The response of arctic $\Delta R_{sfc,alb}$ is similar as that of $\Delta R_{TOA,alb}$ (Figure 5b). Similar to the response of Arctic $\Delta R_{TOA,Ta}$, the Arctic $\Delta R_{sfc,Ta}$ response is also strong (Figure 5c), but the signs of $\Delta R_{sfc,Ta}$ responses are generally opposite from those of $\Delta R_{TOA,Ta}$ response. Notably, the response of Arctic $\Delta R_{sfc,Ts}$ to tropical ocean warming is significantly greater than that of $\Delta R_{TOA,Ts}$. The sign of Arctic $\Delta R_{sfc,Ts}$ is opposites to that of Arctic $\Delta R_{sfc,Ta}$, but they exhibit similar spatial distributions (Figure 5d). This indicates that an increase in Ta leads to radiative warming to the surface, but the surface loses more energy by emitting more thermal radiation after the surface is warmed up. The responses of Arctic $\Delta R_{sfc,LH}$ and Arctic $\Delta R_{sfc,SH}$ are negative in response to warmings in the tropical Pacific and positive in response to warmings in the tropical Indian Ocean (Figure 5e, f); however, these responses are relatively small, suggesting that these factors have a limited impact on Arctic ΔR_{sfc} .

Similar to the Arctic regions, the contribution of cloud to Antarctic ΔR_{sfc} is also negligible (Figure 5g). Albedo has no significant impact on Antarctic ΔR_{sfc} (Figure 5h), because sea ice concentration is fixed in these patch experiments and snow cover in the Antarctica does not change significantly in these experiments. Ta and Ts are the main contributors to Antarctic ΔR_{sfc} , with Antarctic $\Delta R_{sfc,Ta}$ responding positively and Antarctic $\Delta R_{sfc,Ts}$ responding negatively to tropical ocean warming (Figure 5i, j). The responses of Antarctic $\Delta R_{sfc,LH}$, and $\Delta R_{sfc,SH}$ are minimal (Figure 5k, l). These results suggest that while temperature adjustments are notable in Antarctica, responses of cloud cover and surface heat fluxes to remote SST warming have a small impact on Antarctic ΔR_{sfc} .



185 **Figure 5: Difference of annual mean $\Delta R_{sfc,cld}$ (a), $\Delta R_{sfc,alb}$ (b), $\Delta R_{sfc,Ta}$ (c), $\Delta R_{sfc,Ts}$ (g), ΔR_{LH} (h), ΔR_{SH} (i) for Arctic and annual mean $\Delta R_{sfc,cld}$ (d), $\Delta R_{sfc,alb}$ (e), $\Delta R_{sfc,Ta}$ (f), $\Delta R_{sfc,Ts}$ (j), ΔR_{LH} (k), ΔR_{SH} (l) for Antarctica between conjugate warming and cooling patch experiments.**



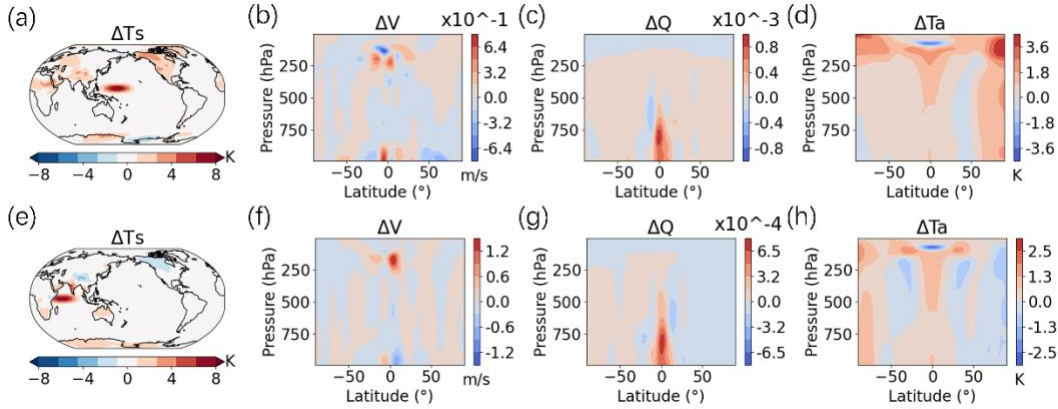
3.2 AHT responses to Regional SST Changes

190 According to Figures. (4-5), air temperature change is the primary contributor to PEB responses in these experiments. The sign of ΔR_{adv} is generally same as $\Delta R_{sfc, Ta}$, and oppsite from $\Delta R_{TOA, Ta}$. In addition, the difference between TOA and surface energy budget reflects the contribution of changes in polar AHT. Therefore, AHT plays a critical role in determining PEB by changing the air temperature of polar regions. The responses of AHT to SST perturbations in the midlatitudes are consistent with our intuition, but the opposite Arctic AHT responses to SST warming over the tropical Indian Ocean and tropical Pacific
195 Ocean requires further investigations.

To explore the underlying mechanisms of this phenomenon, we compared the climate responses to warmings in two illustrative patches within the tropical Pacific Ocean (TPO) and Indian Ocean (TIO). The center of the illustrative TPO patch is (180°E, 0°), and the center of the illustrative TIO is (60°E, 0°).

The responses of surface temperature (ΔT_s), meridional wind (ΔV), air temperature (ΔT_a), and humidity (ΔQ) to warmings in
200 these patches are presented in Figure 6, which provide background information to later AHT studies. In response to warmings in the illustrative TPO region, the response of zonal mean meridional wind is significant in the tropical and subtropical regions, but small at high latitudes. Near the surface around 10°S, as well as at 250 hPa in the upper atmosphere between the equator and 20°S, there is a significant northerly wind anomaly. However, at 100 hPa in the upper atmosphere near 10°S, there is a southerly wind anomaly (Figure 6b). There is a significant increase in ΔQ in the northern hemisphere from the surface up to
205 550 hPa (Figure 6c). In terms of ΔT , warming begins at the surface around 0° and extends upwards to 100 hPa, then propagates towards the poles, and there is an air temperature increase in the Arctic regions (Figure 6d). The increase of Arctic air temperature is a result of enhanced AHT to Arctic regions, which leads to a radiative heating to the surface and radiative cooling to the TOA fluxes.

In response to warmings in the illustrative TIO region, there are southerly wind anomalies at the surface around 10°N, while
210 at higher altitudes, northerly wind anomalies prevail (Figure 6f). ΔQ increases in the southern hemisphere, but decreases in the northern hemisphere, indicating a decrease of meridional latent heat transport near 60°N. TIO warming results in a cooling effect in the Arctic, which is induced by the decrease of AHT to the Arctic regions (Figure 6h).



215 **Figure 6: The spatial distribution of ΔT_s response (a) following an increase in SST over the TPO, along with the zonal mean profiles of ΔV (b), ΔQ (c), and ΔT_a (d), compared to the spatial distribution of ΔT_s response (e) after an increase in SST over the TIO, and the zonal mean profiles of ΔV (f), ΔQ (g), and ΔT_a (h).**

To quantify the impacts of SST warming over the TPO and TIO on the Arctic AHT, we computed the AHT responses to the warming of the two patches separately. AHT can be calculated as the vertically integrated and zonally averaged transport of moist static energy (S). According to Neelin and Held (1987), S can be defined as follows:

$$S = c_p T_a + LQ + gZ, \quad (5)$$

where T_a represents atmospheric temperature, c_p is the specific heat capacity of air at constant pressure, L denotes the latent heat of vaporization of water, Q is specific humidity, g is the acceleration due to gravity, and Z represents geopotential height.

225 The components of S will be denoted below by S_T , S_Z , and S_Q .

The poleward transport of moist static energy S can be decomposed into mean meridional circulation (MOC), stationary eddy (SE), transient eddy (TE), and transient overturning circulation (TOC) components, following the methodologies of Priestley (1948) and Lorenz (1953). According to Donohoe (2020), for each latitude θ , atmospheric energy transport is:

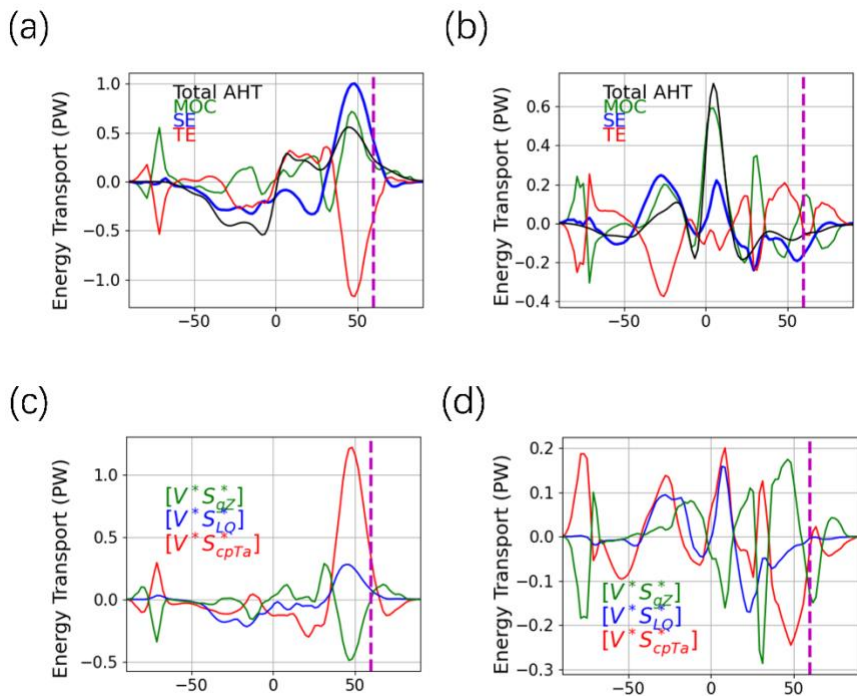
$$AHT(\theta) = 2\pi a \cos(\theta) \int_0^{P_s} [\bar{V}][\bar{S}] + [\overline{V^* S^*}] + [\overline{V' S'}] + [\overline{V'}][\bar{S}'] \frac{dp}{g}, \quad (6)$$

230 where V represents the meridional velocity. Square brackets $[\dots]$ denote zonal averages, overbars $\overline{(\dots)}$ denote time averages over each month of analysis, asterisks $(\dots)^*$ are departures from the zonal average, and primes $(\dots)'$ are departures from the time average. The first term signifies the MOC driven by the vertical gradient in S , taking into account mass conservation in MOC energy transport. The second term is SE, showing poleward transport in warm or moist sectors. These first two terms are derivable from monthly mean data. The third term pertains to the transport associated with TE, primarily baroclinic synoptic eddies. The fourth term involves energy transport by the covariance between zonal-mean overturning circulation



and vertical stratification, referred to as TOC, which is significantly smaller than the other components and thus often excluded in AHT discussions.

Figure 7 shows the changes in AHT and its components in response to warmings in the TPO and TIO. AHT response to warmings in TPO at 60°N is positive, and AHT response to warmings in TIO at 60°N is negative. For both cases, AHT to the Arctic region is dominated by SE (Figure 7b), and the opposite SE response to TPO and TIO leads to opposite responses in AHT, which also causes different responses of TOA and surface energy budgets in the Arctic regions. Additionally, Figures. 7(c) and (d) further dissect the SE responses to warmings in the TPO and TIO, respectively, and the results indicates that dry static energy predominantly drives the SE response to warmings in both TPO and TIO.



245

Figure 7: Decomposition of meridional AHT. (a) and (b) display the changes in meridional AHT following SST warming in the TPO and TIO, respectively. The total AHT is represented by a thick black line, while the contributions from the MOC, SE, and TE are depicted by fine lines in green, blue, and red, respectively. Panels (c) and (d) detail the decomposition of the SE component from (a) and (b), with the contributions from Z, Q, and T shown in green, blue, and red, respectively. The purple dotted line represents the 60°N latitude line.

250

To better understand the opposite response of SE heat flux to warmings in TPO and TIO, we analyzed the spatial distribution of SE heat fluxes. Following the approach outlined by Yohai Kaspi (2013), the calculation of SE heat flux denoted as V^*S^* involves the direct subtraction of zonal and time mean components:



255 $V^*S^* = \overline{VS} - [\overline{V}][\overline{S}]$, (7)

and the vertically integrated SE heat flux (ϕ) can be computed through the following integral:

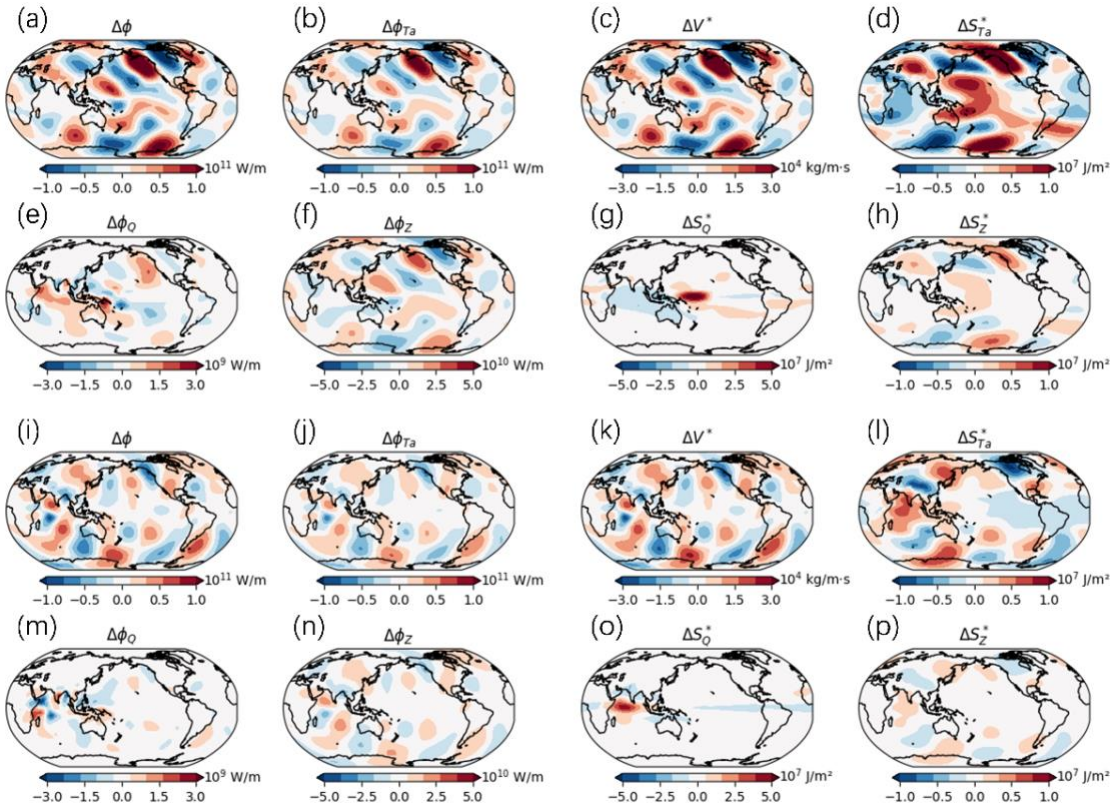
$$\phi = \int_0^{P_s} V^*S^* \frac{dp}{g}, \quad (8)$$

In response to warmings in the TPO, the vertically integrated SE heat flux exhibits significant oscillatory characteristics over the Pacific Ocean. According to Figure 8(a), ϕ increases in the western tropical Pacific, decreases over the north-west and
260 central Pacific, and then increases again over the northeastern Pacific and Alaska. Over land, ϕ decreases over north-east Asia, increases over the Tibetan Plateau and Europe. This phenomenon is consistent to Goss (2016), who found that warming in the low-latitude Pacific leads to increased ϕ in higher latitudes.

Combining Eq. (7) and Eq. (10), we are able to further attribute ϕ to changes in dry static heat flux ($\Delta\phi_{Ta}$), latent heat flux ($\Delta\phi_Q$), and potential energy ($\Delta\phi_Z$), respectively. Among the three main contributing factors to $\Delta\phi$, $\Delta\phi_{Ta}$ aligns closely with
265 the overall $\Delta\phi$ pattern, indicating it as the primary contributor (Figure 8b). The spatial pattern of $\Delta\phi_{Ta}$ can be explained by the change of ΔV^* and ΔS_{Ta}^* (Figure 8c-d), which reflects the spatial pattern of stationary waves. In addition, $\Delta\phi_Q$ is large in the low latitudes, but is small near the poles (Fig. 8e). The $\Delta\phi_Z$ pattern is also similar to $\Delta\phi$ but with lower values (Fig. 8f). The spatial pattern of $\Delta\phi_Q$ and $\Delta\phi_Z$ can be understood by the change of ΔV^* , ΔS_Q^* and ΔS_Z^* (Figures 8c, g, h).

In response to warmings in the TIO, the spatial pattern of $\Delta\phi$ oscillation is quite different from the TPO case. The transfer of
270 SE heat flux encounters obstacles near the Tibetan Plateau, which might explain why the response of $\Delta\phi$ is different in the Northern hemisphere and the Southern hemisphere. $\Delta\phi_{Ta}$ remains dominant, $\Delta\phi_Q$'s contribution is low, and $\Delta\phi_Z$ mirrors the $\Delta\phi$ pattern (Figs. 8i-n).

Based on these results, we are able to understand why the responses of AHT near 60°N to warmings in TPO and TIO are different. TPO warming triggers local northward SE, leading to significant energy fluctuation amplitude in the mid-to-high
275 latitude Pacific, thereby enhancing meridional energy flow northward. This mechanism facilitates the influx of warm, moist air into the Arctic, ultimately causing Arctic warming. Conversely, in the TIO, the Tibetan Plateau effects the poleward propagation of SE in the tropical warm pool, and the SE responses finally leads to Arctic cooling. These findings support the research results of Goss (2016) and the tropical excitation mechanism for Arctic warming outlined by Lee et al. (2011).



280 **Figure 8:** (a) $\Delta\phi$ induced by SST warming in the TPO. (b) The contribution of $\Delta\phi_{Ta}$ to the SE. (c) The vertical
integration of ΔV^* from the surface to the TOA. (d) The vertical integration of ΔS_{Ta}^* from the surface to the TOA. (e)
The contribution of $\Delta\phi_Q$ to the SE. (f) The contribution of $\Delta\phi_Z$ to the SE. (g) The vertical integration of ΔS_Q^* from
the surface to the TOA. (h) The vertical integration of ΔS_Z^* from the surface to the TOA. (i) Same as (a) but for the
TIO. (j) Same as (b) but for the TIO. (k) Same as (c) but for the TIO. (l) Same as (d) but for the TIO. (m) Same as (e)
285 but for the TIO. (n) Same as (f) but for the TIO. (o) Same as (g) but for the TIO. (p) Same as (h) but for the TIO.

3.3 Reconstruction of polar energy budget based on the Green's function approach

The response of PEB to regional SST changes might be used to qualitatively explain how SST variations affect PEB.

290 The sensitivity of the PEB to SST perturbations within a specific grid box, identified by index i , can be estimated using the
following equation (Zhou et al. 2017):

$$\left(\frac{\partial R}{\partial SST_i}\right)_p = \frac{\sum_p \Delta SST_p \left(\frac{\partial R}{\partial SST_i}\right)_p}{\sum_p \Delta SST_p} = \frac{\partial R}{\partial SST_p} \frac{S_i}{S_p}, \quad (9)$$



where R denotes a specific energy flux, S_i and S_p represent the ocean surface area of the specific grid point and the patch, respectively, and ΔSST_p is the SST anomaly in the p th patch [Eq. (1), noting that ΔSST_p equals zero for grid points outside of a patch], and SST_i denotes the SST in the i th grid box. $\left(\frac{\partial R}{\partial SST_i}\right)_p$ reflects the average response of R to a 1 K increase in SST

295 within a specific grid box inside the patch. Additionally, $\frac{\partial R}{\partial SST_p}$ illustrates the variation in the PEB per unit of patch-averaged SST change, derived from experiments involving conjugate ± 1 K patch warming. The sensitivity for grid boxes within a single patch corresponds to the average R change due to a 1 K warming within that specific grid box. For grid boxes overlapping multiple patches, the sensitivity is determined by the weighted average value $\left(\frac{\partial R}{\partial SST_i}\right)_p$. The sensitivities of PEB to SST perturbation in each grid box are shown in Figure 9.

300 Utilizing these sensitivities, we can reconstruct the PEB response to arbitrary changes in SST through the Green's function approach, represented as:

$$\Delta R = \sum_i \frac{\partial R}{\partial SST_i} \Delta SST_i + \varepsilon_i, \quad (10)$$

where ε_i is an error term, which represents the contributions from nonlinearities and non-SST induced factors.

Then we use the Green's function approach to reconstruct the AHT in response to 8 different SST patterns in the EOF-SST experiments (Figures. 10a-h), and the Green's function reconstructed AHT are then compared to model-produced values in the EOF-SST experiments (Figures. 10i-j). The results show that the majority of the experimental simulations of ΔR_{adv} align closely with the ΔR_{adv} reconstructed by the Green's function, lying near the $y = x$ line. The biases of the Green's function reconstructed values are partially induced by the SST change inside the Arctic region, which is not captured by the Green's function reconstruction, and non-linear terms also contribute to the bias. Therefore, the Green's function approach can

310 qualitatively explain how the SST perturbation patterns in Figure 10(a-h) affects PEB.

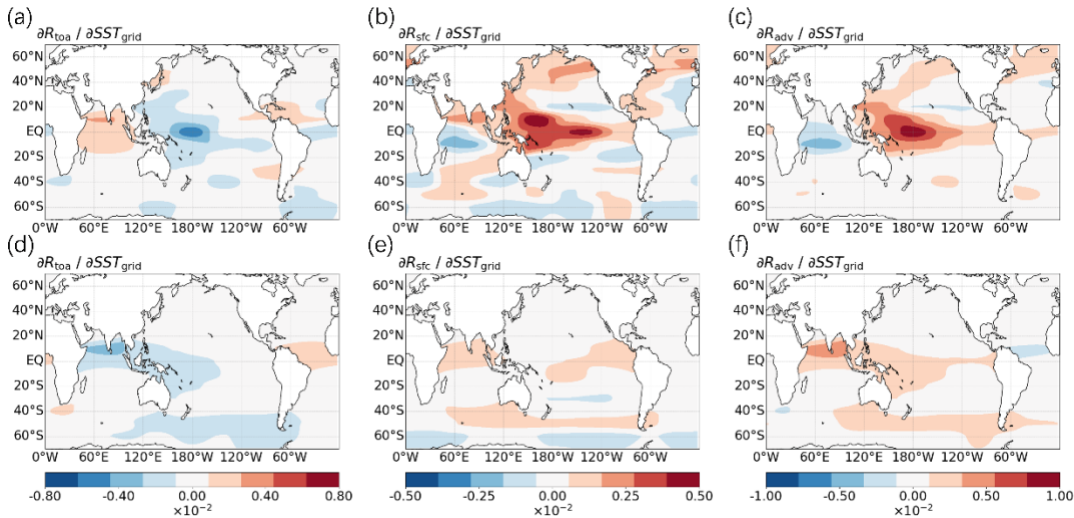
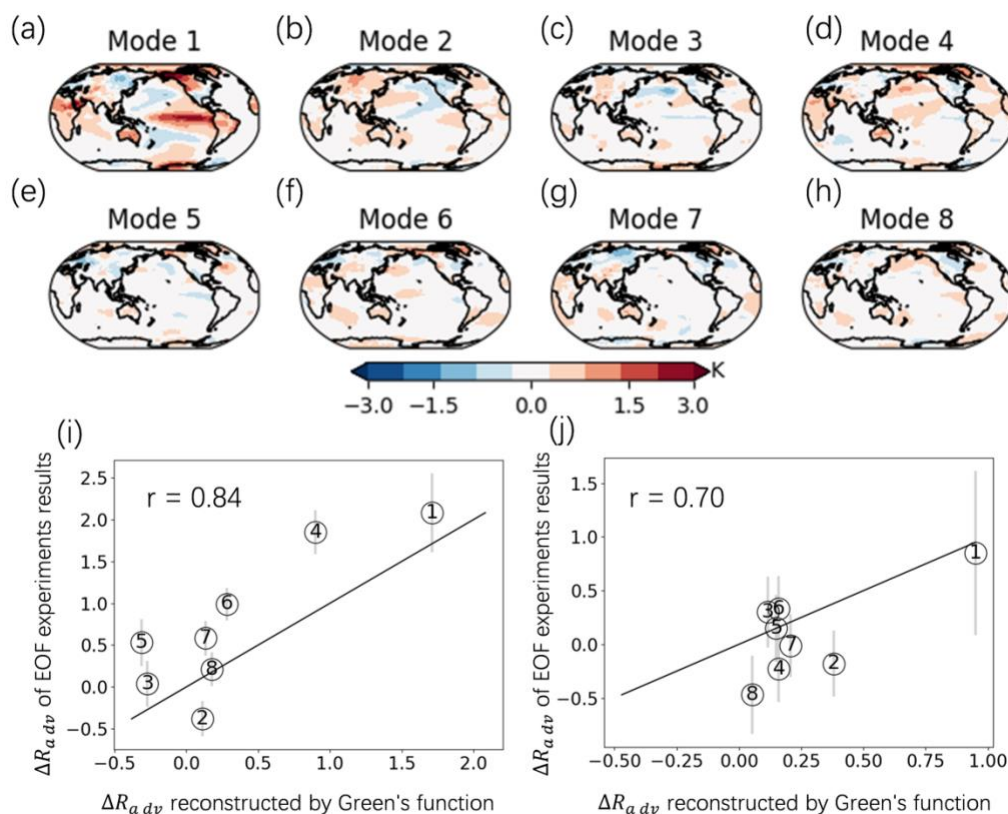


Figure 9: The sensitivity of (a) $\partial R_{toa}/\partial SST_i$ of Arctic, (b) $\partial R_{sfc}/\partial SST_i$ of Arctic, (c) $\partial R_{adv}/\partial SST_i$ of Arctic, (d) $\partial R_{toa}/\partial SST_i$ of Arctic, (e) $\partial R_{sfc}/\partial SST_i$ of Arctic, (f) $\partial R_{adv}/\partial SST_i$ of Antarctica to surface warming in each grid box, calculated using Eq. (9). The units are $W/m^2/K$.

315



320

Figure 10: (a-h) The surface temperature change patterns in individual EOF-SST experiments. (i) Comparison of Arctic ΔR_{adv} responses to different SST change patterns in EOF-SST experiments (y-axis) and that reconstructed by the Green's function approach (x-axis). The digits represent the number of corresponding EOF modes in each experiment. Error bars correspond to the 95 % confidence interval. (j) Response of Antarctica ΔR_{adv} .

4 Conclusion

This study delves into the mechanisms behind the responses of radiative budget in high-latitude regions to sea surface warmings in the low latitudes through a series of idealized SST change experiments. It elucidates the mechanisms through which the PEB responds to distant SST variations, revealing significant different impacts of SST changes across different oceanic regions on the Arctic and Antarctic energy budgets. These impacts are mediated by alterations in AHT, the

325

distribution of sensible heat flux from stationary eddies, and the interactions among various climatic drivers such as temperature, humidity, and cloud radiative processes.

Specifically, increases in SST in the Pacific and Indian Oceans have opposing effects on the Arctic PEB in Boreal winter, attributable to different responses of stationary waves to warming in these oceans, which subsequently alter the patterns of poleward AHT. Warming in the Pacific SST tends to enhance heat transport to the Arctic, leading to Arctic air temperature increases, whereas warming in the Indian Ocean diminishes the heat transport towards the Arctic, resulting in Arctic air temperature decreases. Additionally, the study highlights that the response of the PEB varies with the season. During Boreal winter, the sensitivity of the Arctic PEB to SST changes in tropical regions is stronger, indicating a higher sensitivity of the polar region to tropical ocean warming in winter. Using radiative kernels, the contributions of meteorological factors to the TOA radiation response were quantified. The results indicate that air temperature change is the primary contributor to changes in polar TOA radiation, while the contributions from clouds and albedo are relatively smaller. The decomposition of surface radiation also shows that air temperature and surface temperature are the main contributors to changes in polar surface radiation. Finally, the study reconstructed the AHT responses under different EOF-SST modes using the Green's function approach, validating the consistency between the model experiment results and the Green's function reconstructions. Although biases exist in certain EOF modes, partially due to SST changes within the polar regions and non-linear effects, the Green's function method generally provides a reasonable reconstruction of the PEB response to SST changes.

The primary findings of the study are summarized as follows:

1. In response to SST warmings in most tropical and midlatitude regions, polar air temperatures increase due to enhanced AHT, leading to an increase in the polar surface energy budget and a decrease in the polar TOA energy budget.
2. The response of Arctic AHT to warmings in the tropical Indian Ocean is negative in Boreal winter. Stationary eddies play a crucial role in modulating the polar AHT response to global SST changes.
3. Subtropical SST changes have relatively weak impacts on the polar energy budget.

The findings of this study have significant implications for understanding and predicting polar climate responses to global warming. We find that the distinct responses of the Arctic and Antarctic energy budgets to regional SST changes underscore the necessity of considering regional specificity when modeling and predicting climate change. Our findings emphasize the critical role of radiative feedbacks in shaping the polar climate, providing insights that could enhance the accuracy of climate models. The differential impacts of SST changes in various oceanic regions on the polar energy budgets highlight the importance of incorporating regional specificity in climate models. Accurate modeling of these impacts is crucial for reliable climate projections. Moreover, the study underscores the pivotal role of AHT in modulating polar temperatures. Understanding the mechanisms of AHT and its interaction with stationary eddies can lead to improved predictions of polar climate responses to global SST changes. The analysis of radiative feedbacks, including the roles of temperature, humidity, and clouds, provides a comprehensive understanding of the factors contributing to polar amplification. This knowledge can be utilized to refine radiative transfer models and enhance their predictive capabilities.



360 **Author Contributions**

Methodology: Chen Zhou;

Investigation: Qingmin Wang;

Writing – original draft preparation: Qingmin Wang;

Writing – review & editing: Chen Zhou, Yinchun Liu, Lujun Zhang.

365

Code Availability

The code used in this study are available upon request from the corresponding author.

Acknowledgements

370 This work is supported by NSFC 42375038.

Competing interests

The contact author has declared that none of the authors has any competing interests.

References

- 375 Alexeev, V. A., Langen, P. L., and Bates, J. R.: Polar amplification of surface warming on an aquaplanet in “ghost forcing” experiments without sea ice feedbacks, *Clim. Dyn.*, 24, 655–666, <https://doi.org/10.1007/s00382-005-0018-3>, 2005.
- Baggett, C. and Lee, S.: An identification of the mechanisms that lead to Arctic warming during planetary-scale and synoptic-scale wave life cycles, *J. Atmos. Sci.*, 74, 1859–1877, <https://doi.org/10.1175/JAS-D-16-0156.1>, 2017.
- Barsugli, J. J. and Sardeshmukh, P. D.: Global atmospheric sensitivity to tropical SST anomalies throughout the Indo-Pacific basin, *J. Clim.*, 15, 3427–3442, [https://doi.org/10.1175/1520-0442\(2002\)015<3427>2.0.CO;2](https://doi.org/10.1175/1520-0442(2002)015<3427>2.0.CO;2), 2002.
- 380 Barton, N. P., Klein, S. A., Boyle, J. S., and Zhang, Y. Y.: Arctic synoptic regimes: Comparing domain-wide Arctic cloud observations with CAM4 and CAM5 during similar dynamics., 117, D15205, <https://doi.org/10.1029/2012JD017589>, 2012.
- Boeke, R. C. and Taylor, P. C.: Seasonal energy exchange in sea ice retreat regions contributes to differences in projected Arctic warming, *Nat. Commun.*, 9, 5017, <https://doi.org/10.1038/s41467-018-07061-9>, 2018.



- 385 Budyko, M. I.: The effect of solar radiation variations on the climate of the Earth, *Tellus*, 21, 611–619, <https://doi.org/10.3402/tellusa.v21i5.10109>, 1969.
- Cao, G. and Zhang, G. J.: Role of vertical structure of convective heating in MJO simulation in NCAR CAM5.3, *J. Clim.*, 30, 7423–7439, <https://doi.org/10.1175/JCLI-D-16-0913.1>, 2017.
- Chung, C. E. and Räisänen, P.: Origin of the Arctic warming in climate models, *Geophys. Res. Lett.*, 38, L21704, <https://doi.org/10.1029/2011GL049816>, 2011.
- 390 Dickinson, R. E., Meehl, G. A., and Washington, W. M.: Ice-albedo feedback in a CO₂-doubling simulation, *Climatic Change*, 10, 241–248, <https://doi.org/10.1007/BF00143904>, 1987.
- Donohoe, A., Armour, K. C., Roe, G. H., Battisti, D. S., and Hahn, L.: The partitioning of meridional heat transport from the last glacial maximum to CO₂ quadrupling in coupled climate models, *J. Clim.*, 33, 4141–4165, <https://doi.org/10.1175/JCLI-D-19-0797.1>, 2020.
- 395 Duan, L., Cao, L., and Caldeira, K.: Estimating contributions of sea ice and land snow to climate feedback, *J. Geophys. Res. Atmos.*, 124, 199–208, <https://doi.org/10.1029/2018JD029093>, 2019.
- Fletcher, C. G. and Kushner, P. J.: The role of linear interference in the annular mode response to tropical SST forcing, *J. Clim.*, 24, 778–794, <https://doi.org/10.1175/2010JCLI3735.1>, 2011.
- 400 Goss, M., Feldstein, S. B., and Lee, S.: Stationary wave interference and its relation to tropical convection and Arctic warming, *J. Clim.*, 29, 1369–1389, <https://doi.org/10.1175/JCLI-D-15-0267.1>, 2016.
- Graversen, R. G. and Burtu, M.: Arctic amplification enhanced by latent energy transport of atmospheric planetary waves, *Q.J.R. Meteorol. Soc.*, 142, 2046–2054, <https://doi.org/10.1002/qj.2802>, 2016.
- Hahn, L. C., Armour, K. C., Zelinka, M. D., Bitz, C. M., and Donohoe, A.: Contributions to polar amplification in CMIP5 and CMIP6 models, *Front. Earth Sci.*, 9, 710036, <https://doi.org/10.3389/feart.2021.710036>, 2021.
- 405 Hall, A.: The Role of Surface Albedo Feedback in Climate, *J. Clim.*, 17, 1550–1568, [https://doi.org/10.1175/1520-0442\(2004\)017<1550>2.0.CO;2](https://doi.org/10.1175/1520-0442(2004)017<1550>2.0.CO;2), 2004.
- Kaspi, Y. and Schneider, T.: The role of stationary eddies in shaping midlatitude storm tracks, *J. Atmos. Sci.*, 70, 2596–2613, <https://doi.org/10.1175/JAS-D-12-082.1>, 2013.
- 410 Lañé, A., Yoshimori, M., and Abe-Ouchi, A.: Surface Arctic amplification factors in CMIP5 models: Land and oceanic surfaces and seasonality, *J. Clim.*, 29, 3297–3316, <https://doi.org/10.1175/JCLI-D-15-0497.1>, 2016.
- Lee, S., Gong, T. T., Johnson, N. C., Feldstein, S. B., and Pollard, D.: On the possible link between tropical convection and the Northern Hemisphere Arctic surface air temperature change between 1958 and 2001, *J. Clim.*, 24, 4350–4367, <https://doi.org/10.1175/2011JCLI4003.1>, 2011.
- 415 Lee, S.: Testing of the Tropically Excited Arctic Warming Mechanism (TEAM) with Traditional El Niño and La Niña, *J. Clim.*, 25, 4015–4022, <https://doi.org/10.1175/JCLI-D-12-00055.1>, 2012.
- Lee, S.: A Theory for Polar Amplification from a General Circulation Perspective, *Asia-pacific J. Atmos. Sci.*, 50, 31–43, <https://doi.org/10.1007/s13143-014-0024-7>, 2014.



- 420 Lenssen, N. J. L., Schmidt, G. A., Hansen, J. E., Menne, M. J., Persin, A., Ruedy, R., et al.: Improvements in the GISTEMP uncertainty model, *J. Geophys. Res. Atmos.*, 124, 6307–6326, <https://doi.org/10.1029/2018JD029522>, 2019.
- Li, Z.-X. and Le Treut, H.: Cloud-radiation feedbacks in a general circulation model and their dependence on cloud modelling assumptions, *Clim. Dyn.*, 7, 133–139, <https://doi.org/10.1007/BF00211155>, 1992.
- Li, X., Cai, W., Meehl, G.A. et al. Tropical teleconnection impacts on Antarctic climate changes. *Nat Rev Earth Environ.*, 2, 680–698, <https://doi.org/10.1038/s43017-021-00204-5>, 2021
- 425 Lorenz, E. N.: Available potential energy and the maintenance of the general circulation, *Tellus*, 7, 157–167, 1955.
- Marshall, J., Scott, J. R., Armour, K. C., Campin, J.-M., Kelley, M., and Romanou, A.: The ocean's role in the transient response of climate to abrupt greenhouse gas forcing, *Clim. Dyn.*, 44, 2287–2299, <https://doi.org/10.1007/s00382-014-2308-0>, 2015.
- Mitchell, J. F. B., Senior, C. A., and Ingram, W. J.: CO₂ and climate: a missing feedback?, *Nature*, 341, 132–134, 430 <https://doi.org/10.1038/341132a0>, 1989.
- Neale, R. B., and Coauthors: Description of the NCAR Community Atmosphere Model (CAM 5.0), <https://doi.org/10.5065/D6N877R0>, 2012.
- Neelin, J. D. and Held, I. M.: Modeling tropical convergence based on the moist static energy budget, *Mon. Weather Rev.*, 115, 3–12, [https://doi.org/10.1175/1520-0493\(1987\)115<0003>2.0.CO;2](https://doi.org/10.1175/1520-0493(1987)115<0003>2.0.CO;2), 1987.
- 435 North, G. R.: Theory of Energy-Balance Climate Models, *J. Atmos. Sci.*, 32, 2033–2043, 2007.
- Park, H.-S., Kim, S.-J., Seo, K.-H., Stewart, A. L., Kim, S.-Y., and Son, S.-W.: The impact of Arctic sea ice loss on mid-Holocene climate, *Nat. Commun.*, 9, 4571, <https://doi.org/10.1038/s41467-018-07068-2>, 2018.
- Priestley, C. H. B.: Dynamical control of atmospheric pressure: II—the size of pressure systems, *Q. J. R. Meteorol. Soc.*, 74, 67–72, <https://doi.org/10.1002/qj.49707431908>, 1948.
- 440 Pithan, F., Medeiros, B., and Mauritsen, T.: Mixed-phase clouds cause climate model biases in Arctic wintertime temperature inversions, *Clim. Dyn.*, 43, 289–303, <https://doi.org/10.1007/s00382-013-1964-9>, 2014.
- Rodgers, K. B.: A tropical mechanism for Northern Hemisphere deglaciation, *Geochem.Geophys.Geosyst.*, 4, 1046, <https://doi.org/10.1029/2003gc000508>, 2003.
- Salzmann, M.: The polar amplification asymmetry: Role of Antarctic surface height, *Earth Syst. Dynam.*, 8, 323–336, 445 <https://doi.org/10.5194/esd-8-323-2017>, 2017.
- Sellers, W. D.: A Global Climatic Model Based on the Energy Balance of the Earth-Atmosphere System, *J. Appl. Meteorol.*, 8, 392–400, [https://doi.org/10.1175/1520-0450\(1969\)008<0392>2.0.CO;2](https://doi.org/10.1175/1520-0450(1969)008<0392>2.0.CO;2), 1969.
- Sejas, S. A., Cai, M., Hu, A., Meehl, G. A., Washington, W., and Taylor, P. C.: Individual feedback contributions to the seasonality of surface warming, *J. Clim.*, 27, 5653–5669, <https://doi.org/10.1175/JCLI-D-13-00658.1>, 2014.
- 450 Sejas, S. A., and Cai, M.: Isolating the Temperature Feedback Loop and its Effects on Surface Temperature, *J. Atmos. Sci.*, 73, 3287–3303, <https://doi.org/10.1175/JAS-D-15-0287.1>, 2016.



- Semmler, T., Pithan, F., and Jung, T.: Quantifying two-way influences between the Arctic and mid-latitudes through regionally increased CO₂ concentrations in coupled climate simulations, *Clim. Dyn.*, 54, 3307–3321, <https://doi.org/10.1007/s00382-020-05171-z>, 2020.
- 455 Shaw, T. A. and Tan, Z.: Testing latitudinally dependent explanations of the circulation response to increased CO₂ using aquaplanet models, *Geophys. Res. Lett.*, 45, 9861–9869, <https://doi.org/10.1029/2018GL078974>, 2018.
- Smith, D. M., Screen, J. A., Deser, C., Cohen, J., Fyfe, J. C., García-Serrano, J., et al.: The Polar Amplification Model Intercomparison Project (PAMIP) contribution to CMIP6: Investigating the causes and consequences of polar amplification, *Geosci. Model Dev.*, 12, 1139–1164, <https://doi.org/10.5194/gmd-12-1139-2019>, 2019.
- 460 Solomon, A., Shupe, M. D., Persson, O., Morrison, H., Yamaguchi, T., Caldwell, P. M., et al.: The sensitivity of springtime Arctic mixed-phase stratocumulus clouds to surface-layer and cloud-top inversion-layer moisture sources, *J. Atmos. Sci.*, 71, 574–595, <https://doi.org/10.1175/JAS-D-13-0179.1>, 2014.
- Stuecker, M. F., Bitz, C. M., Armour, K. C., Proistosescu, C., Kang, S. M., Xie, S.-P., et al.: Polar amplification dominated by local forcing and feedbacks, *Nat. Clim. Change*, 8, 1076–1081, <https://doi.org/10.1038/s41558-018-0339-y>, 2018.
- 465 Taylor, P. C., Kato, S., Xu, K. M., and Cai, M.: Covariance between Arctic sea ice and clouds within atmospheric state regimes at the satellite footprint level, *J. Geophys. Res. Atmos.*, 120, 12656–12678, <https://doi.org/10.1002/2015JD023520>, 2015.
- Wang, M., Peng, Y., Liu, Y., Liu, Y., Xie, X., and Guo, Z.: Understanding cloud droplet spectral dispersion effect using empirical and semi-analytical parameterizations in NCAR CAM5.3, *Earth Space Sci.*, 7, e2020EA001276, <https://doi.org/10.1029/2020EA001276>, 2020.
- 470 Vargas Zeppetello, L. R., Donohoe, A., and Battisti, D. S.: Does surface temperature respond to or determine downwelling longwave radiation?, *Geophys. Res. Lett.*, 46, 2781–2789, <https://doi.org/10.1029/2019GL082220>, 2019.
- Yoshimori, M., Abe-Ouchi, A., and Laîné, A.: The role of atmospheric heat transport and regional feedbacks in the Arctic warming at equilibrium, *Clim. Dyn.*, 49, 3457–3472, <https://doi.org/10.1007/s00382-017-3523-2>, 2017.
- Yu, Y., Taylor, P. C., and Cai, M.: Seasonal variations of Arctic low-level clouds and its linkage to sea ice seasonal variations, *J. Geophys. Res. Atmos.*, 124, 12206–12226, <https://doi.org/10.1029/2019JD031014>, 2019.
- 475 Zhou, C., Zelinka, M. D., and Klein, S. A.: Analyzing the dependence of global cloud feedback on the spatial pattern of sea surface temperature change with a Green’s function approach, *J. Adv. Model. Earth Syst.*, 9, 2174–2189, <https://doi.org/10.1002/2017MS001096>, 2017.
- Zhou, J., Lu, J., Hu, Y., and Zelinka, M. D.: Responses of the Hadley circulation to regional sea surface temperature changes, *J. Clim.*, 33, 429–441, <https://doi.org/10.1175/JCLI-D-19-0315.1>, 2020.
- 480